

Minimum distance mapping using three-dimensional optical coherence tomography for glaucoma diagnosis

Boris Považay

Bernd Hofer

Boris Hermann

Angelika Unterhuber

Cardiff University
School of Optometry and Vision Sciences
Biomedical Imaging Group
Cardiff, Wales CF24 4LU
United Kingdom

and

Medical University of Vienna
Center for Biomedical Engineering and Physics
Waehringerstrasse 13
Vienna A-1090, Austria

James E. Morgan

Cardiff University
School of Optometry and Vision Sciences
Biomedical Imaging Group
Cardiff, Wales CF24 4LU
United Kingdom

Carl Glittenberg

Susanne Binder

Rudolf Foundation Clinic Vienna
Department of Ophthalmology
Ludwig Boltzmann Institute
Vienna A-1090, Austria

Wolfgang Drexler

Cardiff University
School of Optometry and Vision Sciences
Biomedical Imaging Group
Cardiff, Wales CF24 4LU
United Kingdom

and

Medical University of Vienna
Center for Biomedical Engineering and Physics
Waehringerstrasse 13
Vienna A-1090, Austria

1 Introduction

Glaucoma remains one of the most common causes of vision loss worldwide, and patient numbers are expected to increase within the coming decade.¹⁻³ In this disease, accelerated retinal ganglion cell death results in dramatic loss of the visual field. Retinal ganglion cells lie at the inner border of the retina and send their processes (axons), covered by support cells (glia), via the retinal nerve fiber layer (the most superficial layer of the retina) toward the optic nerve and successively the brain. To exit the eye, axons pass through a series of collagenous plates (the lamina cribrosa) that are contiguous with the sclera, the collagenous coat of the eye. As retinal

Abstract. Objective imaging of the optic nerve structure has become central to the management of patients with glaucoma. There is an urgent need in diagnosis and staging for reliable objective precursors and markers. Three-dimensional ultrahigh-resolution frequency domain optical coherence tomography (3D UHR OCT) holds particular promise in this respect since it enables volumetric assessment of intraretinal layers including tomographic data for the retinal nerve fiber layer (RNFL) and optic nerve head. The integrated analysis of this information and the resolution advantage has enabled the development of more informative indices of axonal damage in glaucoma compared with measurements of RNFL thickness and cup-to-disc ratio provided by commercial OCT devices. The potential for UHR OCT in enabling the combined analysis of tomographic and volumetric data on retinal structure is explored. A novel parameter was developed; the three-dimensional minimal distance as the optical correlate of true retinal nerve fiber layer thickness around the optic nerve head region. For the purposes of this pilot study, we present data from a normal subject and from two patients with characteristic optic nerve and retinal nerve fiber layer changes secondary to glaucoma. © 2007 Society of Photo-Optical Instrumentation Engineers. [DOI: 10.1117/1.2773736]

Keywords: ophthalmology; tomography; 3D-imaging; image analysis; microscopy; coherent optics.

Paper 06335SSR received Nov. 17, 2006; revised manuscript received Mar. 30, 2007; accepted for publication Apr. 6, 2007; published online Sep. 10, 2007.

ganglion cells die, the associated loss of the axon results in thinning of the retinal nerve fiber layer. At the opening in the sclera (the optic disc), nerve fiber layer thickness increases as axons from the more peripheral retinal areas pass over those from areas closer to the optic disc. Towards the edge of the disc, axons form the neuroretinal rim, with the central area of the disc being devoid of axons, thereby forming a cup-shaped depression known clinically as the optic disc cup. Axon loss, as found in glaucoma, changes the shape of the cup; the neuroretinal rim is thinned and the volume of the cup increases.

Clinically, these early changes can be detected from the remodeling of the glial support tissues that lie within the retinal nerve fiber layer. With white light this process can be detected as wedge or slit-like defects within the nerve fiber

Address all correspondence to: Wolfgang Drexler, Maindy Road, CF24 4KU Cardiff, Wales, United Kingdom. Tel: +44 2920 870 549; Fax: +44 2920 870 608; E-mail: drexlerw@cardiff.ac.uk

layer, where the darker axons are partially substituted by brighter glia. At the neuroretinal rim, this loss results in thinning of the whole layer. Later stages of the disease are often associated with changes within the scleral part of the lamina cribrosa with posterior bowing and compression of the cribrosal plates and deepening of the optic cup.

Although clinical assessment of the optic disc and retinal nerve fiber layer can provide valuable information in the diagnosis of glaucoma, the subjectivity of this assessment limits its application in the detection of early disease or progressive damage. For this reason, many recent studies have focused on the development of methods of improving the quantification of retinal nerve fiber layer (RNFL or NFL) thickness. Historically, this parameter has been described by expressing the vertical dimension optic cup as a ratio of the cup and disc (C/D). The C/D was introduced as a parameter⁴ in standard fundus photography to provide a single value that indicated the degree of glaucomatous optic nerve damage. In the derivation of the C/D, Elschnig's ring is easily seen as the border of the optic disc. Measuring the width of the neuroretinal rim has proven more difficult, reflecting the difficulties associated with boundary definitions on a curved surface that varies considerably between (normal) eyes. Confocal scanning laser ophthalmoscopy has been developed to provide detailed three-dimensional (topographic) maps of the retinal surface. Quantification of retinal nerve fiber layer thickness is made by measurement of the distance between surface topography at the margin of the optic disc⁵ and a reference plane that lies below the retinal surface plot, based on known values of retinal nerve fiber layer thickness. RNFL measurements with this technique are therefore indirect and vulnerable to changes in the orientation of the margin of the optic disc (defined as the opening in the scleral trough which the axons run to form the optic nerve) relative to the retinal surface. In some eyes in which the plane of the optic disc is tilted⁶ or skewed,⁷ anatomically or pathologically,⁸ topographic measurements are not made orthogonal to the retina surface, and assumptions about the relationship between RNFL thickness and the retinal surface contour are invalid. Other devices, such as the scanning laser polarimeter (clinically known as the GDx), have attempted to overcome these problems by using a surrogate estimate of RNFL thickness, based on the birefringent properties of retinal ganglion cell axons. Since the degree of birefringence varies as a function of RNFL thickness this can provide an index of RNFL thickness that can be compared to the topographic techniques.⁹ Unfortunately, the relationship between true histological thickness and birefringence is also unreliable, even when account is taken of changing confounding corneal birefringence around the optic disc.¹⁰

By comparison, optical coherence tomography (OCT), which is based on interferometric depth ranging, can provide delineation of intraretinal layers and allow quantification of the RNFL¹¹ without the need for an arbitrary reference plane^{12–15} and can even give access to spatially resolved birefringence information.¹⁶ Clinical OCT devices provide high-resolution cross-sectional images of the retinal nerve at the margin of the optic disc.^{15,17} The interpretation of these images is commonly based on legacy methods for the analysis of the retinal nerve fiber layer in which the retinal nerve fiber layer thickness is measured relative to a reference plane, usually placed at the margin of the optic disc. This geometric

estimate of RNFL represents a marked improvement over confocal or polarimetric techniques but remains vulnerable to the effects of optic disc tilt and deformations.

More recently, the development of extremely sensitive¹⁸ and therefore fast frequency domain (spectral) OCT techniques^{19–21} that use a different data acquisition technique (similar to optical frequency domain reflectometry)²² coupled with ultrahigh-resolution OCT²³ has for the first time raised the possibility for true three-dimensional (3D) quantification of the retinal nerve fiber layer thickness (Fig. 1). This imaging modality provides clear delineation of the retinal nerve fiber layer relative to retinal landmarks^{24,25} such as the scleral rim. Since a 3D model of the optic nerve head (ONH) can be derived, it is possible to develop novel parameters that better approximate the cross-sectional areas of the retinal nerve fiber layer and therefore a better index, which acts as an improved indicator for the degree of retinal ganglion cell loss in glaucoma.

In this paper, we describe the derivation of new parameters—the minimum distance map (MDM) and the minimum circumpapillary band (MCB) for the robust quantification of RNFL thickness. The NFL-MDM thickness map is derived by calculating the geometrical minimum distance between the upper and lower orders of the NFL for every point on the inner retinal surface. An MCB is a circumpapillary band with the smallest area that is spanned through the NFL from the inner to the outer NFL surface and encloses the optic disc. The smallest MCB is commonly situated at the proximity of the scleral rim, and its area is strongly correlated with absolute axon content. With UHR-OCT, the scleral rim can be identified and provides an invariant landmark for the analysis of the optic disc in glaucoma. The key difference between this and earlier methods for NFL quantification is that the angle of the connection line between the inner retinal surface and the scleral rim varies as a function of the retinal surface tilt and true NFL thickness. The parameter therefore represents a true Euclidean, rather than the projected measure of NFL thickness. The detailed derivation of these parameters is described in the methodology for this study, and results are then presented based on the analysis of normal and glaucomatous optic discs.

2 Methods

2.1 Derivation of a 3D Optic Nerve Head Model

Ideally, measurements of RNFL thickness made orthogonal to the axon path should provide the most accurate measure of the axon population. Figure 2 shows typical cross-sectional (superior–inferior) scans of the ONH, visualizing the situation. To minimize error, thickness measurements should be made at a point in the retina where the RNFL thickness is maximal in respect to other tissue. Since this represents the point of greatest convergence where the entire axon population can be assessed, the density is high, causing a high signal contrast. The situation is modeled in 3D in Fig. 3. In the top graph, an analytical result based on the continuity of material (assuming a constant average axon+glia cross section) shows the increasing NFL thickness when approaching the optic disc, caused by the 3D geometry (the same amount of tissue has to fit into a smaller circumpapillary area). Detailed histological analysis of the retinal nerve fiber layer indicates that

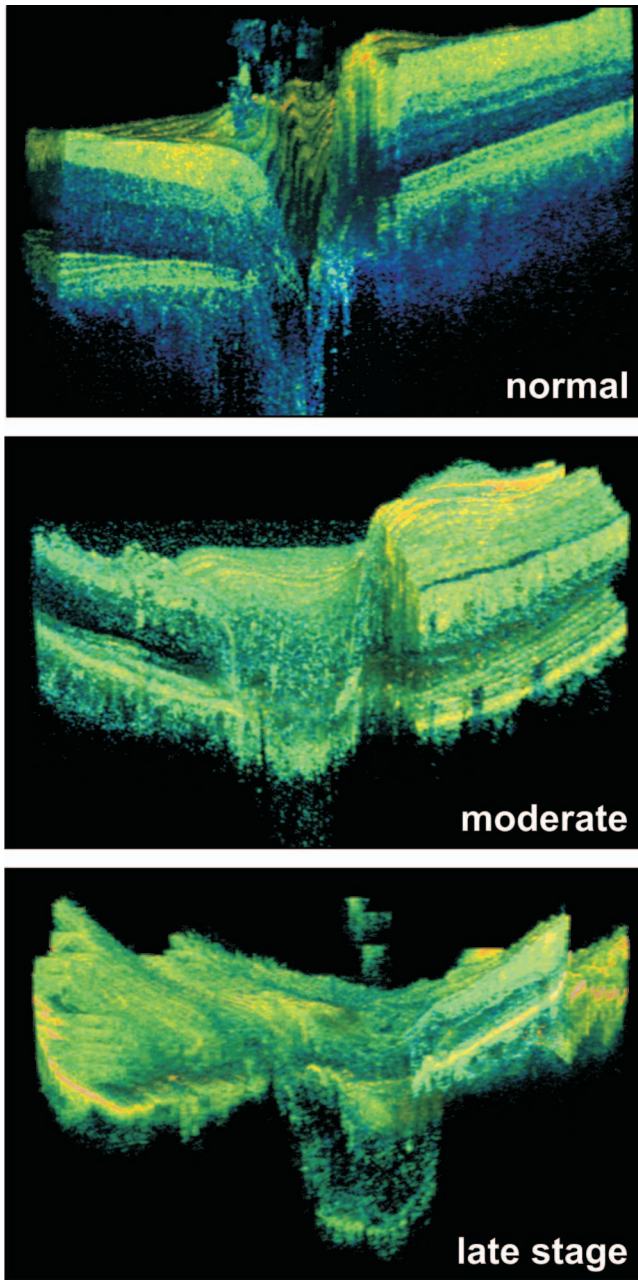


Fig. 1 3D visualization of high-speed ultrahigh-resolution optical coherence tomography providing topographic information. Normal ONH (top, $3 \times 3 \times 1.3 \text{ mm}^3$); intermediate stage glaucoma (middle, C/D: 1.02, $4.5 \times 4.5 \times 1.3 \text{ mm}^3$); advanced glaucoma (bottom, C/D: 0.56). The different elevation of the papilla is clearly visible. The position of the lamina cribrosa in the center is successively displaced, and the relative amount of material passing into the scleral canal is changing.

individual axons vary in diameter (at a microscopic scale) along their length. However, when considered as a population, these effects are negligible and it is reasonable to assume an overall invariant axon diameter. Also, all individual axons do not always take the most direct path toward the optic disc when viewed from within the retinal plane,^{26,27} caused by unequal distribution of axons and the tendency to optimize the path length in 3D space or by local turbulence. This has only

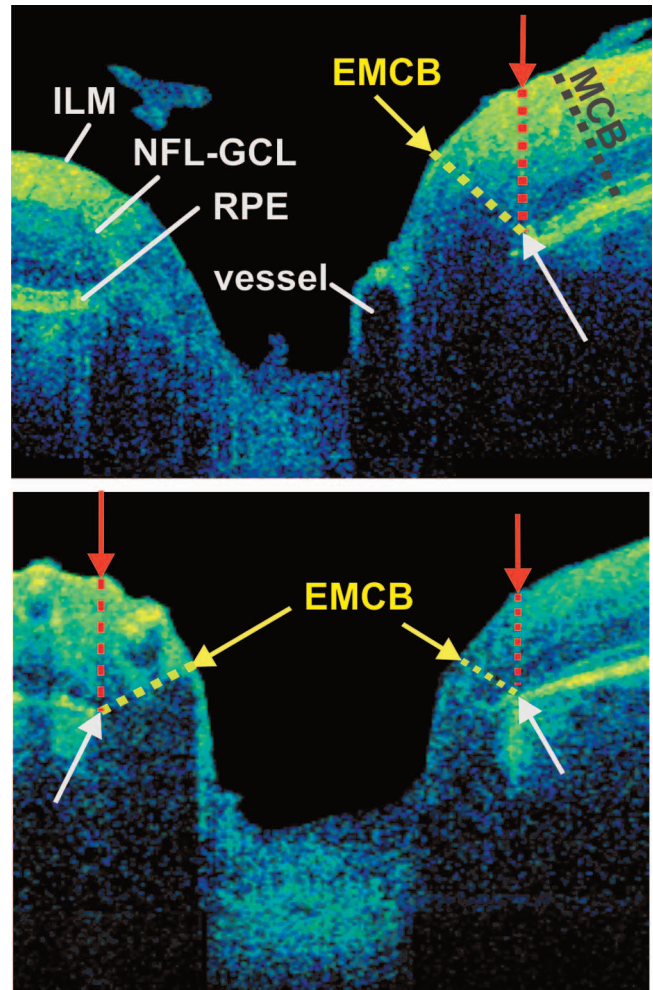


Fig. 2 Cross-sectional view of normal ONH (top) and ONH with glaucoma (bottom). White arrows point to the scleral (Elschnig's) ring. Here only the two-dimensional (2D) distance is used to form the circumpapillary bands (MCB). Red arrows and dashed lines indicate the projected thickness, while the yellow ones depict the scleral border within this 2D OCT scan, forming a part of the MCB attached to Elschnig's ring (EMCB).

a small impact on the new measures, and the assumption that the axons as an ensemble take the shortest route to the optic disc is still valid. Inside the margin, assuming a constant density of axons leaving through the optic nerve, the model predicts a linearly decreasing NFL thickness. Outside the margin of the disc, the cross sections are oriented almost orthogonally to the retinal surface. By definition, these cross sections describe a closed circumpapillary band spanning the whole NFL thickness and enclosing the papilla, but with the smallest possible area content at the given average distance from the papilla. This is a strict geometrical consequence of orthogonality to the average fiber orientation, which also prohibits circumpapillary bands that are tilted or skewed in this respect. Mathematically, the axons are treated similarly to a laminar, non-rotating, and incompressible fluid with negligible turbulence, and the cross section can be described as a static solution of the equation of continuity or, in terms of fluid dynamics, as the Navier–Stokes equations. These minimal circumpapillary bands (MCB, blue regions in the green section of Fig. 3) are

approximated and examined further by circumpapillary scans in conventional slow-scanning time domain OCT. When approaching the optic nerve, three effects alter the geometry of these bands of equal area much stronger than the side effects mentioned above: first, the thickening of the NFL; second, the change of thickness and morphology of the underlying tissue, which is strongly reduced toward Elschnig's scleral ring and even more at the optic nerve itself, third, the changing relative axon/glia diameter ratio. Hence, the overall retinal topography does not resemble the extremely sharp peaking as prognosticated by the idealized model showing the thickness, rather than the absolute vertical extent, although it is usually quite visible at the nasal quadrant.

The main problem of the current 2D approaches is the low specificity to detect the outer NFL-retinal ganglion cell interface (NFL-GCL) border at the margin and the tilt of the whole tissue, including the optic disc and its 3D shape. Due to the lack of information on the real axon orientation, the correct tilt of the MCB cannot be derived from any of the data sets, including 3D UHR-OCT. Therefore, extraction of the MCB at this position, neglecting the scleral structure, as well as the morphology of the other tissue make this 2D indicator intrinsically unreliable and lead to an arbitrary circumpapillary band that resembles the correct 3D shape in a vague approximation only. On the other hand, the definition of pathological changes will be seen first in the smallest of all MCBs, because there the axon density will prevail. For a simple model of a normal with constant axon/glia ratio, this can be restricted to allow only for constant hydrodynamic flow, leading to a constant area of the MCBs (Fig. 3 normal) and the characteristic culmination at the margin of the cup. Under stress, however, this ratio is affected by thinning and reduction of glial tissue, similar to an increase in flow. Successively, we propose to find the MCB with the smallest area that can be found in the proximal region of the ONH, marked in Fig. 2 as EMCB, where the axon concentration is supposed to be maximized and the local axon orientation already is close to parallel, like in the optic nerve. As a pathognomonic parameter, the relation between this area and the rather unchanged cross section of the neuronal tissue at the lamina cribrosa is suggested. This information can be derived from the volumetric data that are currently only available with 3D UHR-OCT by following the maximum flow model (which is essentially based on Bernoulli's principle) originally derived for calculation of the highest flow of an incompressible fluid through an arbitrary lumen.

2.2 Image Acquisition System

3D raster-scanned OCT measurements were performed with a fiber optic, ultrahigh-resolution system with a Titanium:Sapphire laser (Femtolasers Integral, Vienna, Austria) operating at 800 nm with 150-nm bandwidth, capable of 3 μm axial resolution that was already utilized in other clinical studies.²⁴ The signal was acquired in a spectrometer setup by a 2048 pixel line scan camera (Atmel Aviiiva), capable of up to a 29 kHz line rate. The scanning components were built upon the Zeiss OCT-2 patient module with modifications to account for the broader spectral bandwidth. Sixty consecutive OCT B-mode scans with 1024 \times 1024 pixels were collected from a 4.5 \times 4.5- or 3 \times 3-mm³ region of the ONH. Tomograms were acquired from three subjects with different stages of

glaucoma and normal subjects with good transparency of the ocular media. For the purpose of this pilot study, 2 typical glaucoma eyes with moderately advanced disease and one normal eye are displayed from a wider range of patients with different pathologies. The study was approved by the Ethics Committee of the City of Vienna, Austria, and conducted according to the tenets of the Declaration of Helsinki (final revision: 52nd WMA General Assembly, Edinburgh, Scotland, 2000). Written and informed consent was obtained from all study participants after detailed explanation of the aims and risks of the study.

2.3 Postprocessing Procedure

After spectral resampling and Fourier transformation, the cross-sectional slices were shifted according to their cross correlation to compensate for motion artifacts. Segmentation of the different layers was performed by distinguishing the texture of different layers and their interfaces. The search was started by finding the first signal above a threshold and the strongest signals in every depth scan, identifying the internal limiting membrane (ILM) when starting from the vitreous, and the RPE when starting from the opposite side of the tomogram (scleral side). The RPE is absent at most points around the scleral rim, which allows it to be automatically detected as a discrete ring whose inner border marks the boundary of the optic disc. The place of this ring is coincident with the scleral one so that it effectively appears as a hole in the scleral sheet through which the axons pass. The retinal nerve fiber layer surface can easily be identified in all images. The first texture underlying this is the NFL-retinal ganglion cell interface, which is also mostly well defined (Figs. 1 and 2). The positional information of the ILM, NFL-GCL, and RPE planes was stored as depth values in a $3 \times n \times m$ matrix covering all nm depth scans. An optimized global minimum search algorithm was used to find the nearest voxel of the ILM in 3D space and assigned this distance as the minimum distance mapping (MDM) value of the resulting surface matrix. To keep continuity between the 3D points of the mesh, spline algorithms were utilized.

Volumetric information of the 3D topographic data set was then compiled using Matlab to produce standard difference maps, projected in the imaging direction as well as to compute minimum 3D distance maps and to color-code the extracted MDM data. For quantification of the scleral rim's shape, the 3D data points were connected by a 3D spline and smoothed by least-square fitting and minimization of the spline order. Following the maximum flow model, the associated MDM measured from the ILM surface was found by automated search within the two surfaces and successively the minimum circumpapillary band at Elschnig's ring (EMCB), containing the minimum nerve fiber cross section, and its area was calculated. The disc rim does not lie on a simple plane but is curved in 3D space furthermore and often tilted in respect to the extrapolated scleral plane. Our hypothesis states that in case of glaucoma the natural balance of nerve fibers to the other material is altered in relative disadvantage of the NFL, which especially affects the EMCB. As suggested earlier, this can be diagnosed by comparing the quasi-unchanged area of the scleral canal with the strongly altered MCB area. During our tests, the scleral ring was more strongly distorted

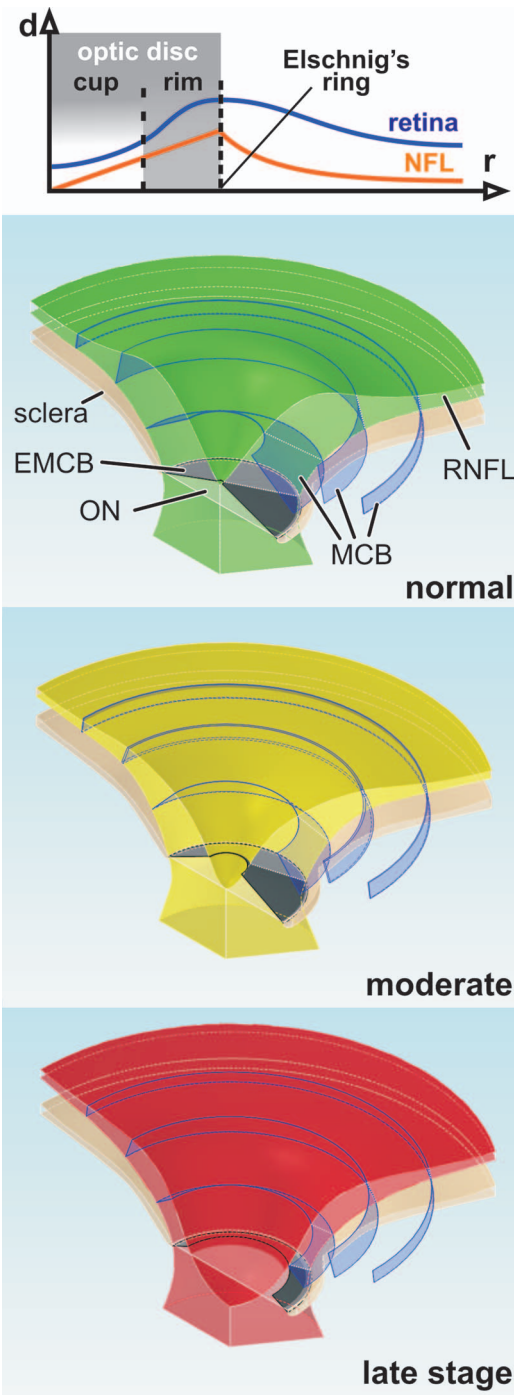


Fig. 3 Top: Modeled thickness (d) of the NFL (orange) and total retinal thickness (blue) versus radius (r) assuming a flat sclera, centered at the ONH. In the periphery, NFL thickness (in orange) rises according to a square law until the first bundles can exit to the optic nerve at Elschnig's ring (dashed line) at a constant rate, leading to a linear reduction of thickness towards the center. Due to support tissue the overall retinal thickness changes are smoother. Mid to bottom: Models of three different states of glaucoma. Sclera displayed in brown. While in the normal case all NFL-MCB cross-sections (blue) are equally large as the corresponding cross-section of the optic nerve and the cupping ends above the scleral rim, the later stages depict a lower minimum ratio between the area of the minimum circumpapillary band that is attached to Elschnig's ring EMCB (black) to the minimum cross section of the optic nerve at the lamina cribrosa (ON, white). For visualization the retinal material is removed at a wider angle.

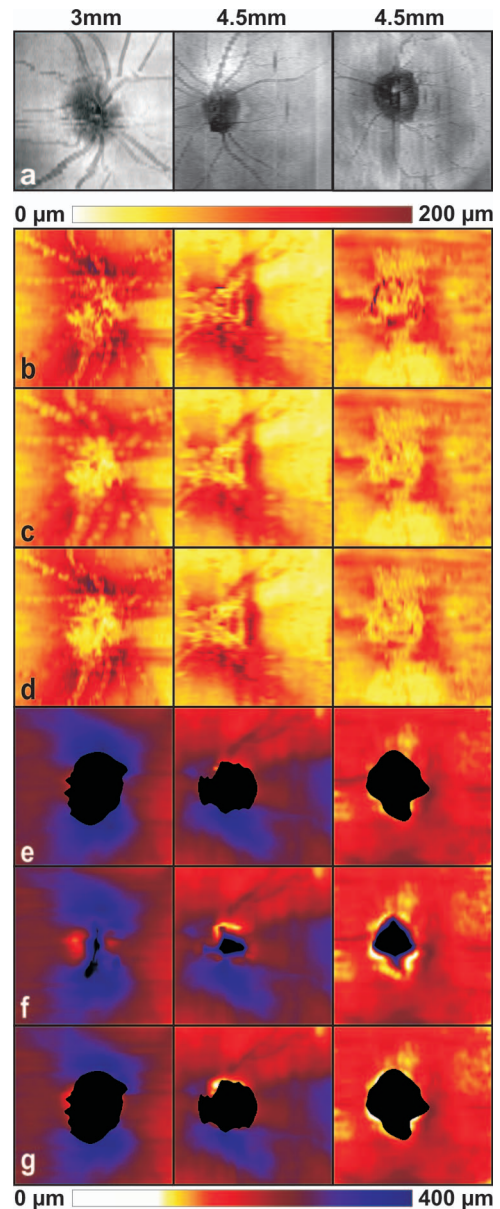


Fig. 4 2D views of the retinal maps for normal (left—transversal scanning range, 3 mm), intermediate glaucoma (middle—4.5 mm), and advanced glaucoma (right—4.5 mm). Nerve fiber layer and retinal thickness are color-coded. (a) reconstructed fundus image at 800 nm, calculated as an integration across the depth over the volume acquired by OCT. (b) Standard mapping of the nerve fiber layer (NFL) thickness, as indicated in Fig. 2. (c) Minimum distance map (MDM) of the NFL calculated for every point on the ILM. (d) NFL-MDM at the bottom of the NFL. (e) Projected retinal thickness map. (f) Retinal thickness MDM measured from the ILM. (g) Retinal thickness MDM at retinal pigment epithelium (RPE).

in glaucomatous eyes than in the normal case, which might be an indicator as well, but this would involve a wider longitudinal study.

3 Results and Discussion

Since the reflectivity information of 3D UHR OCT is volumetric, depth information can be integrated to generate fundus images [Fig. 4(a)], which are registered to detailed position

maps of the inner internal limiting membrane (ILM—corresponding to the retinal surface) and the retinal pigment epithelium (RPE—corresponding to the outer retinal surface) around the optic nerve head. In Fig. 4(b), nerve fiber thickness has been rendered as a difference map of the segmented data at the ILM and the NFL-GCL border. In addition, the MDM maps for the NFL were calculated for every point on the ILM surface to the outer NFL surface [Fig. 4(c)] and vice versa [Fig. 4(d)]. Since the segmentation of the NFL-GCL interface is not as reliable as the segmentation of the RPE, due to shadowing effects of large vessels, varying signal quality, and ripples, caused by bundling of the fibers, the full retinal thickness (RT) was calculated by a simple difference calculation between the heights of the two surfaces [Fig. 4(e)]. Furthermore, retinal MDM maps, calculated at the ILM [Fig. 4(f)] as well as at the RPE [Fig. 4(g)], are displayed. The ability for this technique to provide a measure of RNFL thickness is reduced at the margin of the optic disc because the change in the slope of the retinal surface is associated with increased light scatter and a reduced signal-to-noise ratio. Due to limited optical resolution, only the volume or cross section can be calculated from the surfaces, while the individual nerve fiber bundles and their orientation are still below the resolution of current OCT devices. At the margin of the optic disc (i.e., overlying Elschnig's ring), the total retinal thickness approximates the retinal nerve fiber layer thickness since the other retinal layers are absent; the full width of the retina at the scleral rim can therefore be taken as a geometrically relevant correlate for retinal nerve fiber layer thickness.

Color coding of the 3D MDM plot allows visualization of NFL thickness, which is similar to those obtained with devices such as the GDx. As confirmed with histology, the RT-MDM can be used to reveal the peripapillary NFL profile at the margin of the disc.^{11,13} At greater eccentricities, the NFL-MDM (measuring only the NFL thickness instead of the inner and outer surfaces of the complete retina) is more appropriate since the NFL can be segmented more easily with the retina oriented orthogonally to the scanning beam. The physically correct dimension of the minimum nerve fiber cross section enables measurement of the retinal nerve fiber layer's cross-sectional area, even in those eyes with advanced glaucomatous damage as shown in Fig. 4. MDMs of three selected cases are shown as a proof of principle to demonstrate the viability of this new measuring modality as a planar representation. Eyes of a normal subject (Fig. 4, left), a patient with intermediate glaucoma but no visual field loss (C/D: 1.02) and advanced glaucoma (C/D: 0.56) with significant loss of visual field, are presented.

Both the 3D MDM (Fig. 5) and the 2D maps [Figs. 4(c)–4(g)] immediately highlight the difference of the three cases in ways that are clinically accessible. It is interesting to note that the MDMs measured from the ILM to the RPE and vice versa can have a fairly different distribution of values [Figs. 4(f) and 5(e)], especially in pathologic cases, due to the 3D nature of the problem. This means, for instance, that a single close point of one layer will show up as a single bright spot, when measured from this layer, while in the other measurement a wider area will be brighter. Therefore, in the normal case [Figs. 4(f) and 4(g), left] the two planes are well separated, and the thicknesses are almost equally distributed on both maps. Even for the NFL-MDMs, the distribution is

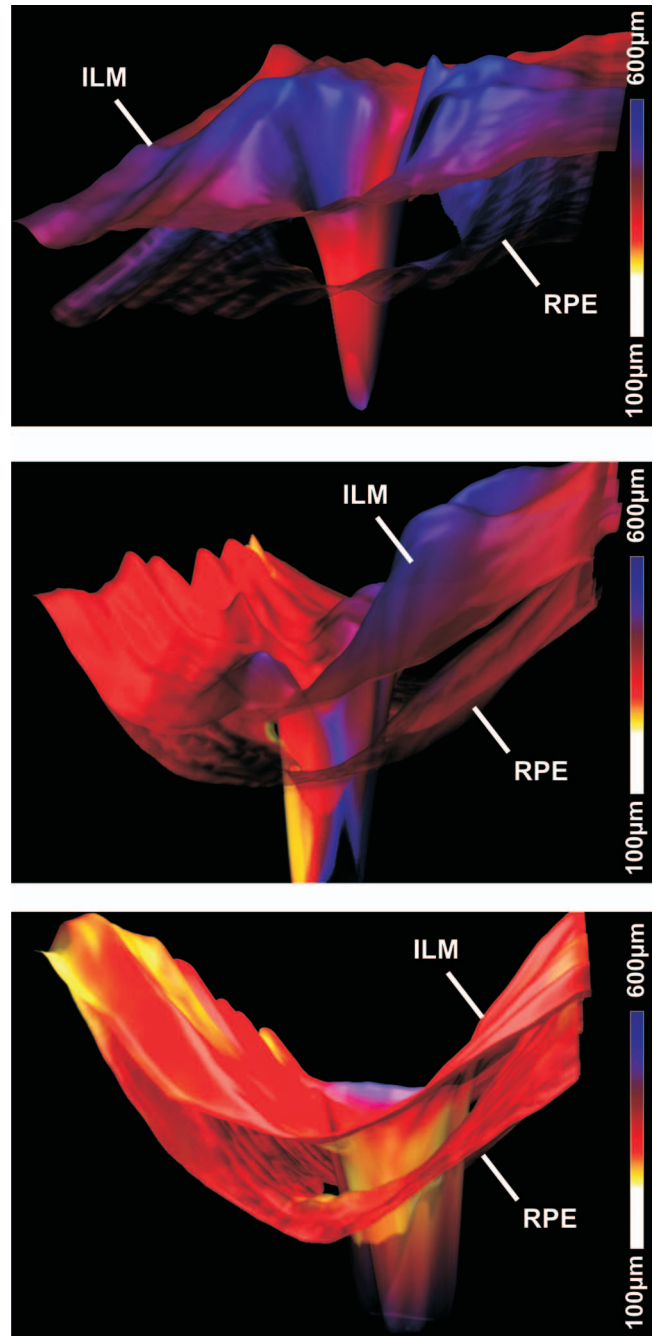


Fig. 5 Three-dimensional renderings of the internal limiting membrane (ILM) and the retinal pigment epithelium (RPE) in each image for a normal subject (top), intermediate glaucoma (middle), and advanced glaucoma (bottom). Colors indicate the three-dimensional minimum distance measured from the respective surfaces and visualize the three-dimensional nature of the problem and indicate local nerve fiber losses as hot-spots. The increasing total cupping with glaucoma progress includes changes of the sclera and affects the vertical thickness, while the true, absolute three-dimensional thickness is unaffected.

rather smooth [Figs. 4(c) and 4(d) left]. A notable difference between the two views depicts the different roughness of the associated layers, suggesting that the ILM is almost planar while the vessels are more situated at the distal side (closer to

Table 1 Calculated areas for three different subjects with progressing stages of glaucoma. The area of the termination of the RPE is compared with the projected (fundus view type) area and the minimum circumpapillary band (MCB) that is tilted in space as well as the projected CB above the scleral rim. Comparison of the relative change of the MCBs to their respective scleral ring areas is given.

Area type		Intermediate Advanced		
		Normal	Glaucoma	Glaucoma
Termination of RPE	(mm ²)	1.11	1.50	2.06
Projected RPE termination	(mm ²)	1.10	1.48	2.03
RT-MCB	(mm ²)	1.32	1.20	0.78
Projected RT-CB	(mm ²)	1.55	1.50	1.02
Rel. RT-MCB	—	+19%	-20%	-62%
Rel. projected	—	+39%	0%	-50%

the RPE) of the NFL. In the advanced pathological case [Figs. 4(f) and 4(g), middle] the absolute distance between the layers is reduced (indicated by a red shift), but also the distribution becomes asymmetric. The neuronal MDM [Figs. 4(c) and 4(d), middle] starts to develop a highly contrasted ring indicating abrupt changes in the thickness probably associated with strong mechanical stress, while the MDM of the retinal thickness still shows smooth characteristics, suggesting a continuous structure. One might also diagnose the abnormal shape of the ring as an indicator for mechanical stress, but this has to be examined in further detail. In the exemplary end-stage glaucoma case [Figs. 4(c) and 4(d), right], the overall NFL thickness is very low and the vessels are clearly visible in both NFL-MDMs. The retina thickness MDM [Figs. 4(f) and 4(g), right] can especially be used as a good indicator in respect to the standard thickness map because of a clearly visible ring pointing out a very strong bend, cupping, and thinning of the tissue. The sharp contrast and enlarged dark region (visualizing the large distance) in the NFL already indicate a deeper structure. Mapping the MDMs within a 3D rendering onto their respective surfaces intuitively demonstrates the reason for the MDMs' colors (Fig. 5) and helps to correlate the reduced thickness within 3D.

Having access to the real 3D data points allows to calculate the real area of the scleral rim and the retinal MDM and permits us to compare them with their projected analogues (as used in other techniques). With flat (normal to the imaging direction) scleral rims, and therefore normal scleral canals, the difference is negligible. For surfaces that are strongly tilted with in respect to the imaging direction, however, the projected thicknesses and areas are misleading and cannot indicate the correct change of retinal thickness loss. In Table 1, the areas of the presented cases are shown together with the values scaled to the scleral rim area. This helps to compensate for individual differences in the scleral canal's diameter and focus onto subjective material loss. These numbers indicate a reasonable advantage when using the 3D MCB to relate it to the glaucoma stage. The normal case shows a relative higher amount in the MCB, while the intermediate case already exhibits an equal thickness in the scleral canal and at the MCB.

In advanced glaucoma, as expected, the relative thickness loss is prominent. The respective projected distances (essentially demarking the cylinder on top of the scleral rim) that can be compared to measurements obtained by RTA and TD-OCT overestimate the amount of retinal material but are relatively constant.

4 Conclusions

Although the presented minimum distance maps have been compared for a limited range of subjects, they have already been shown to give results that are consistent with known histological changes in glaucoma. MDMs provide easily interpretable visualization of local retinal thickness and surface roughness. We anticipate that increased imaging speed will allow higher resolution and isotropic sampling of the ONH and improve the correct estimation of RNFL volumes and areas. The MDM technique appears to be robust and is less sensitive to the confounding effects of optic nerve head tilt than other imaging modalities (e.g., SLO tomography). Further evaluation of this technique is now required in larger clinical studies to the diagnostic precision for the detection of early glaucoma or progressive damage. With the advent of next-generation, high-speed frequency domain OCT systems, accurate 3D evaluation of retinal nerve fiber layer thickness with appropriate transformation for visualization will enable the advantages of 3D OCT to be transferred effectively to the clinical domain.

Acknowledgments

Support for the project was provided by the following institutions: Cardiff University, FP6-IST-NMP-2 STREPT (017128), FWF Y 159-PAT, the Christian Doppler Society, FEMTOLASERS GmbH (Vienna, Austria), and Carl Zeiss Meditec Inc. (Dublin, CA). The authors would also like to thank Harald Sattmann, Medical University Vienna, for technical support and Florian Zeiler and Christiane Falkner-Radler, Department of Ophthalmology, Ludwig Boltzmann Institute, Rudolf Foundation Clinic Vienna, for clinical support.

References

1. H. A. Quigley and A. T. Broman, "The number of people with glaucoma worldwide in 2010 and 2020," *Br. J. Ophthalmol.* **90**(3), 262–267 (2006).
2. J. E. Morgan, H. Uchida, and J. Caprioli, "Retinal ganglion cell death in experimental glaucoma," *Br. J. Ophthalmol.* **84**(3), 303–310 (2000).
3. R. R. Bourne, "Worldwide glaucoma through the looking glass," *Br. J. Ophthalmol.* **90**(3), 253–254 (2006).
4. J. B. Jonas, G. C. Gusek, and G. O. Naumann, "Optic disc, cup and neuroretinal rim size, configuration and correlations in normal eyes," *Invest. Ophthalmol. Visual Sci.* **29**(7), 1151–1158 (1988).
5. C. A. Curcio, P. LE. Saunders, P. W. Younger, and G. Malek, "Peripapillary chorioretinal atrophy: Bruch's membrane changes and photoreceptor loss," *Ophthalmology (Philadelphia)* **107**(2), 334–343 (2000); J. E. Morgan, N. J. Sheen, R. V. North, R. Goyal, S. Morgan, E. Ansari, and J. M. Wild, "Discrimination of glaucomatous optic neuropathy by digital stereoscopic analysis," *Ophthalmology (Philadelphia)* **112**(5), 855–862 (2005).
6. S. D. Piette and R. C. Sergott, "Pathological optic-disc cupping," *Curr. Opin. Ophthalmol.* **17**(1), 1–6 (2006).
7. G. B. Melo, R. D. Libera, A. S. Barbosa, L. M. Pereira, L. M. Doi, and L. A. Melo, Jr., "Comparison of optic disk and retinal nerve fiber layer thickness in nonglaucomatous and glaucomatous patients with high myopia," *Am. J. Ophthalmol.* **142**(5), 858–860 (2006).
8. M. Shimazawa, G. Tomita, T. Taniguchi, M. Sasaoka, H. Hara, Y. Kitazawa, and M. Araie, "Morphometric evaluation of changes with

- time in optic disc structure and thickness of retinal nerve fiber layer in chronic ocular hypertensive monkeys," *Exp. Eye Res.* **82**(3), 427–440 (2006).
9. K. Akiyasu, N.-K. Azusa, F. T. E. Michael, M. Hidetaka, N. Makoto, and N. Akira, "Comparison of confocal scanning laser ophthalmoscopy, scanning laser polarimetry and optical coherence tomography to discriminate ocular hypertension and glaucoma at an early stage," *Graefe's Arch. Clin. Exp. Ophthalmol.* **244**(1), 58 (2006).
 10. J. E. Morgan, A. Waldock, G. Jeffery, and A. Cowey, "Retinal nerve fiber layer polarimetry: histological and clinical comparison," *Br. J. Ophthalmol.* **82**(6), 684–690 (1998).
 11. E. Z. Blumenthal, J. M. Williams, R. N. Weinreb, C. A. Girkin, C. C. Berry, and L. M. Zangwill, "Reproducibility of nerve fiber layer thickness measurements by use of optical coherence tomography," *Ophthalmology* **107**(12), 2278–2282 (2000).
 12. J. S. Schuman, M. R. Hee, C. A. Puliafito, C. Wong, T. Pedutklozman, C. P. Lin, E. Hertzmark, J. A. Izatt, E. A. Swanson, and J. G. Fujimoto, "Quantification of nerve-fiber layer thickness in normal and glaucomatous eyes using optical coherence tomography—a pilot study," *Arch. Ophthalmol. (Chicago)* **113**(5), 586–596 (1995).
 13. J. S. Schuman, T. Pedutklozman, L. Pieroth, E. Hertzmark, M. R. Hee, J. R. Wilkins, J. G. Coker, C. A. Puliafito, J. G. Fujimoto, and E. A. Swanson, "Quantification of nerve fiber layer thickness loss over time in the glaucomatous monkey model using optical coherence tomography," *Invest. Ophthalmol. Visual Sci.* **37**(3), 5255–5255 (1996).
 14. G. Wollstein, L. A. Paunescu, T. H. Ko, J. G. Fujimoto, A. Kowalevicz, I. Hartl, S. Beaton, H. Ishikawa, C. Mattox, O. Singh, J. Duker, W. Drexler, and J. S. Schuman, "Ultrahigh-resolution optical coherence tomography in glaucoma," *Ophthalmology* **112**(2), 229–237 (2005).
 15. B. Cense, T. C. Chen, B. H. Park, M. C. Pierce, and J. F. de Boer, "Thickness and birefringence of healthy retinal nerve fiber layer tissue measured with polarization-sensitive optical coherence tomography," *Invest. Ophthalmol. Visual Sci.* **45**(8), 2606–2612 (2004).
 16. J. F. deBoer, T. E. Milner, M. J. C. vanGemert, and J. S. Nelson, "Two-dimensional birefringence imaging in biological tissue by polarization-sensitive optical coherence tomography," *Opt. Lett.* **22**(12), 934–936 (1997).
 17. G. J. Jaffe, and J. Caprioli, "Optical coherence tomography to detect and manage retinal disease and glaucoma," *Am. J. Ophthalmol.* **137**(1), 156–169 (2004).
 18. M. A. Choma, M. V. Sarunic, C.-H. Yang, and J. A. Izatt, "Sensitivity advantage of swept source and Fourier domain optical coherence tomography," *Opt. Express* **11**(18), 2183–2189 (2003).
 19. R. A. Leitgeb, W. Drexler, A. Unterhuber, B. Hermann, T. Bajraszewski, T. Le, A. Stingl, and A. F. Fercher, "Ultrahigh resolution Fourier domain optical coherence tomography," *Opt. Express* **12**(10), 2156–2165 (2004).
 20. M. Wojtkowski, V. J. Srinivasan, T. H. Ko, J. G. Fujimoto, A. Kowalczyk, and J. S. Duker, "Ultrahigh-resolution, high-speed, Fourier domain optical coherence tomography and methods for dispersion compensation," *Opt. Express* **12**(11), 2404–2422 (2004).
 21. B. Cense and N. A. Nassif, "Ultrahigh-resolution high-speed retinal imaging using spectral-domain optical coherence tomography," *Opt. Express* **12**(11), 2435–2447 (2004).
 22. A. F. Fercher, C. K. Hitzenberger, G. Kamp, S. Y. El-Zaiat, K. Seta, and B. K. Ward, "Measurement of intraocular distances by back-scattering spectral interferometry Interferometric absolute distance measurement utilizing a mode-jump region of a laser diode," *Opt. Commun.* **117**, 43–48 (1995).
 23. W. Drexler, "Ultrahigh-resolution optical coherence tomography," *J. Biomed. Opt.* **9**(1), 47–74 (2004).
 24. U. Schmidt-Erfurth, R. A. Leitgeb, S. Michels, B. Považay, S. Sacu, B. Hermann, C. Ahlers, H. Sattmann, C. Scholda, A. F. Fercher, and W. Drexler, "Three-dimensional ultrahigh-resolution optical coherence tomography of macular diseases," *Invest. Ophthalmol. Visual Sci.* **46**(9), 3393–3402 (2005).
 25. V. J. Srinivasan, M. Wojtkowski, A. J. Witkin, J. S. Duker, T. H. Ko, M. Carvalho, J. S. Schuman, A. Kowalczyk, and J. G. Fujimoto, "High-definition and 3-dimensional imaging of macular pathologies with high-speed ultrahigh-resolution optical coherence tomography," *Ophthalmology* **113**(11), 2054 e2051–2014 (2006).
 26. J. E. Morgan, G. Jeffery, and A. J. Foss, "Axon deviation in the human lamina cribrosa," *Br. J. Ophthalmol.* **82**(6), 680–683 (1998).
 27. T. E. Ogden, "Nerve fiber layer of the macaque retina: Retinotopic organization," *Invest. Ophthalmol. Visual Sci.* **24**(1), 85–98 (1983).